JACS
JOURNAL OF THE AMERICAN CHEMICAL SOCIETY
Article
Cite This: J. Am. Chem. Soc. 2017, 139, 16923-16931
pubs.acs.org/JACS

Collision Dynamics during the Electrooxidation of Individual Silver Nanoparticles

Donald A. Robinson,[†,∥] Yuwen Liu,[†,‡,∥] Martin A. Edwards,[†] Nicholas J. Vitti,[†] Stephen M. Oja,[§] Bo Zhang,[*,§] and Henry S. White[*,†]

[†]Department of Chemistry, University of Utah, Salt Lake City, Utah 84112, United States
[‡]College of Chemistry and Molecular Sciences, Wuhan University, Wuhan, 430072, China
[§]Department of Chemistry, University of Washington, Seattle, Washington 98195-1700, United States

Supporting Information

ABSTRACT: Recent high-bandwidth recordings of the oxidation and dissolution of 35 nm radius Ag nanoparticles at a Au microelectrode show that these nanoparticles undergo multiple collisions with the electrode, generating multiple electrochemical current peaks. In the time interval between observed current peaks, the nanoparticles diffuse in the solution near the electrolyte/electrode interface. Here, we demonstrate that simulations of random nanoparticle motion, coupled with electrochemical kinetic parameters, quantitatively reproduce the experimentally observed multicurrent peak behavior. Simulations of particle diffusion are based on the nanoparticle-mass-based thermal nanoparticle velocity and the Einstein diffusion relations, while the electron-transfer rate is informed by the literature exchange current density for the Ag/Ag^+ redox system. Simulations indicate that tens to thousands of particle−electrode collisions, each lasting ∼6 ns or less (currently unobservable on accessible experimental time scales), contribute to each experimentally observed current peak. The simulation provides a means to estimate the instantaneous current density during a collision (∼500−1000 A/cm^2), from which we estimate a rate constant between ∼5 and 10 cm/s for the electron transfer between Ag nanoparticles and the Au electrode. This extracted rate constant is approximately equal to the thermal collisional velocity of the Ag nanoparticle (4.6 cm/s), the latter defining the theoretical upper limit of the electron-transfer rate constant. Our results suggest that only ∼1% of the surface atoms on the Ag nanoparticles are oxidized per instantaneous collision. The combined simulated and experimental results underscore the roles of Brownian motion and collision frequency in the interpretation of heterogeneous electron-transfer reactions involving nanoparticles.

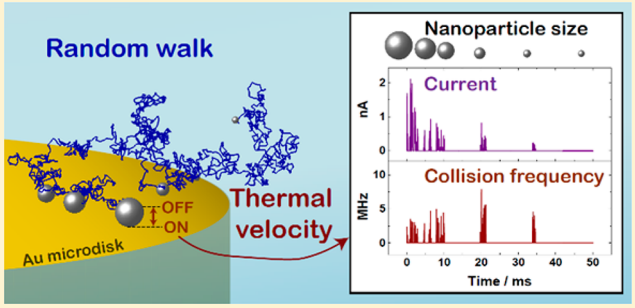

INTRODUCTION

Brownian motion[1] underlies many stochastic processes observed in the physical[2] and life sciences.[3] Some of the earliest experiments investigating Brownian motion involved colloid dispersions.[1b,4] Einstein first applied his microscopic theory of diffusion to the optical experimental results of Svedberg using 25 nm radius Pt colloids.[4b,5] At that time, it was ruled "impossible—at least for ultramicroscopic particles—to ascertain" the instantaneous velocity of a nanoparticle suspended in liquid by direct observation.[5] Significant advances have been made toward this goal in the past decade. For example, Raizen and co-workers have reported the direct measurement of the instantaneous Brownian velocity of a 3 μm silica sphere in air[6] using optical tweezers. In a separate study, the optical trapping method was used again to measure the Brownian displacements of single 1.0 and 2.5 μm silica particles suspended in water with sub-Å resolution on time scales ranging from 10^{-8} to 10^{-3} s, which allowed for determining the time scale of transition from ballistic to diffusive Brownian motion.[7]

An alternative approach to investigate the dynamics of single nanoparticles is through monitoring the current arising from the interaction of electroactive or electrocatalytic nanoparticles with an electrode surface.[8] Since the initial studies of Bard and co-workers,[8] researchers investigating the electrochemical detection of discrete electroactive nanoparticle collisions with microelectrodes have contributed insightful fundamental studies into single nanoparticle electrocatalysis,[9] nanoparticle interactions with bare or modified electrode surfaces,[10] and particle transport/aggregation processes.[11] In many experimental systems studied to date, the nanoparticles simply irreversibly adsorb to the electrode.[11a,g,12] In contrast, in their studies of RuOx nanoparticles interacting with a Au microelectrode, Unwin and co-workers observed clusters of multiple current−time (i−t) peak events and interpreted this behavior to result from multiple collisions of the same electrocatalytic nanoparticle.[13]

Received: September 14, 2017
Published: October 30, 2017

DOI: 10.1021/jacs.7b09842
J. Am. Chem. Soc. 2017, 139, 16923−16931

The collisional behavior of metal nanoparticles at an electrode surface is inherently stochastic. The subject of stochastic behavior in electrochemical systems[14] has grown substantially in recent years as researchers direct their focus toward the electrochemistry of a small number of molecular species[15] and individual nanoparticles.[14c,d,16] Previous electrochemical random walk simulations have focused on outer-sphere one-electron transfer processes involving freely diffusing,[14b] nanogap confined,[17] and tethered redox molecules.[18] In some of these reports, the ET rate constant was directly related to the collisional velocity of the redox molecule, as approximated by the mass-dependent thermal root-mean-square velocity[1a,19] and the probability of electron transfer upon electrode collision.[14b,17,18] Application of this treatment to the experimentally measured kinetically limited rate of ~5 cm/s for the oxidation of ferrocenylmethyltrimethylammonium suggests that an average of ~2000 thermal collisions between the molecule and electrode are required for a single ET event to occur.[14b] Similar stochastic behavior is expected in nanoparticle collision experiments. The charge-transfer kinetics for much larger metal nanoparticles, in contrast, involves much slower collisional velocities (roughly 3−4 orders of magnitude slower due to the large nanoparticle mass relative to a small redox molecule), allowing a longer time for oxidation or reduction to occur. Thus, the transfer of multiple electrons from an electroactive nanoparticle, e.g., Ag, to the electrode substrate is likely to occur during each nanoparticle collision event.[20]

Here we describe a stochastic analysis of the motion and resulting oxidation of 35 nm radius Ag nanoparticles at a Au microelectrode. Oxidation of Ag nanoparticles was first described by Compton and co-workers,[20b] who reported spike-shaped $i-t$ peak events resulting from the collisions of individual citrate-capped Ag nanoparticles (20−50 nm diameter) at a carbon fiber microdisk electrode. In their study, each particle resulted in a *single* peak in the $i-t$ trace, while the average integrated charge for each peak was found to be equal to the predicted value for complete oxidation of the nanoparticle. Kanoufi and co-workers demonstrated a method to optically monitor the transport and electrode reactions of Ag nanoparticles on a Au electrode,[21] and later demonstrated simultaneous optical-electrochemical monitoring of Ag nanoparticle electrodissolution.[22] It was observed that in many cases Ag nanoparticles do not fully oxidize/dissolve upon landing on the electrode surface[22] but rather diffuse into bulk solution after the initial collision.[21] In these prior reports, the experimentally observed current transient for a single Ag nanoparticle oxidation event was typically shown to take the form of a *single* spike-shaped peak. However, we note that the low-pass filters used in these experiments (250 Hz filter)[23] resulted in limited temporal resolution,[20a] and thus, any evidence of multiple collisions from the same Ag nanoparticle would not be directly observable.

Using low-pass filters with higher cutoff frequencies and low-noise instrumentation, we have directly observed that an individual Ag nanoparticle collides many times with a Au microelectrode while undergoing sequential partial oxidations, resulting in a cluster of $i-t$ peak events over an ~25 ms duration.[20a] Examples of representative $i-t$ traces are shown in Figure 1. The durations between consecutive current bursts are on the order of seconds, as shown in the top panel, which suggests that each burst is due to a single particle. In further contrast to previous reports,[20b] we found that citrate-stabilized Ag nanoparticles of 30−35 nm radius undergo only partial

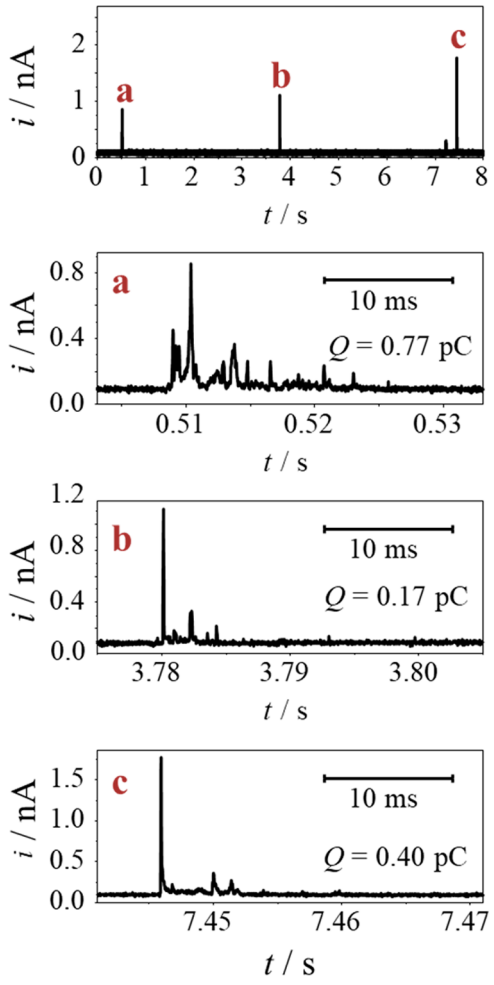

Figure 1. Top panel: experimental $i-t$ trace corresponding to the oxidation of three individual 35 nm radius Ag nanoparticles, labeled a, b, and c, with a 12.5 μm diameter Au microelectrode (shrouded in insulating glass), poised at 0.6 V vs Ag/AgCl quasi-reference electrode (1.1 V vs a standard hydrogen electrode (SHE), see Supporting Information, section 1, for details of experimental procedures). Lower three panels: $i-t$ traces showing that each individual event as labeled in the top panel, plotted on an expanded time scale, consists of a cluster of shorter current peaks. The trace was recorded in an aqueous solution containing 6 mM trisodium citrate and 20 mM KNO_3. A low-pass filter of 10 kHz was applied during acquisition, with a sampling rate of 50 kHz. See Supporting Information, section 2, for additional examples of experimental $i-t$ traces.

(25−50%) oxidation over the time scale of the $i-t$ response. The multipeak current behavior and incomplete nanoparticle oxidation was observed to persist at various concentrations of supporting electrolyte and pH.[20a] Long[24] and Unwin[25] reported very similar multipeak $i-t$ responses for the electrochemical oxidation of single citrate-stabilized Ag particles on both Au[24,25] and C[25] microelectrodes that are consistent with incomplete Ag nanoparticle oxidation for particle sizes ≥30 nm in radius.[24,25] We also discovered that the duration between each peak in a multipeak cluster is significantly affected by the solution viscosity, supporting the hypothesis that the multipeak $i-t$ behavior results from the Brownian motion of the Ag nanoparticle.[20a]

In this Article, we report a 3D lattice random walk simulation of Ag nanoparticle motion with stepwise subnanometer displacements over nanosecond time intervals; these simu-

DOI: 10.1021/jacs.7b09842
J. Am. Chem. Soc. 2017, 139, 16923−16931

lations quantitatively capture the observed electrochemical response of a Ag nanoparticle undergoing repeated collisions with an electrode. Random walk simulations have been reported by Bard,[26] Compton,[16] and Long[24] to model nanoparticle motion and collisions with an electrode. However, these previous simulations of nanoparticle electrochemical collisions have been based on random walk models that employ *arbitrary* step distance and time parameters,[16,24,26] precluding extraction of microscopic ET parameters. We take a different approach by using the nanoparticle mass-dependent thermal velocity to unambiguously describe the nanoparticle motion dynamics. This allows for analysis of the instantaneous current density during a collision, *vide infra*, and thus evaluation of the heterogeneous ET rate constant for Ag nanoparticle oxidation by quantitative comparison with experimental data. We show that the multicollisional Ag nanoparticle oxidation process follows Einstein's theory linking microscopic thermal motion at nanosecond time scales to particle diffusion.[1a] Analysis of this multicollision behavior also suggests that the rate of ET during a nanoparticle/electrode collision is limited by the nanoparticle's thermal velocity.

We developed a three-dimensional lattice random-walk model, shown schematically in Figure 2, to simulate the $i-t$ response for a Ag nanoparticle undergoing dissolution to Ag^+. The blue trace in Figure 2 represents the path taken by the nanoparticle. The larger gray sphere represents the initial particle in solution that diffuses to the surface. In this example, the nanoparticle undergoes three "cluster" sets of oxidation events, denoted as electron transfers in Figure 2, before diffusing away into bulk solution with a reduced size. As detailed below, each of the three "cluster events" consist of hundreds to thousands of microscopic collisions, each contributing to the observed current. As noted above, our simulation accounts for stochastic movement of the Ag nanoparticle based on its mass-dependent thermal velocity.[1] Our model also includes the effect of a finite-size Au microelectrode, as particles that initially collide with the electrode near the electrode/insulator boundary have a high probability of diffusing away from the electroactive Au surface during a real experiment.

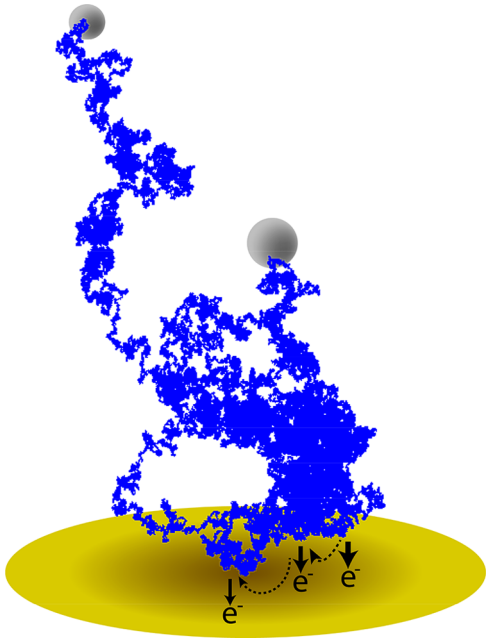

Figure 2. Schematic of a single Ag nanoparticle undergoing electrooxidation at a Au microelectrode (particle and electrode not drawn to scale). The Ag nanoparticle diffuses by a random walk from the bulk solution to the electrode/electrolyte interface on the basis of its mass-dependent thermal velocity (blue trajectory), where it collides with the Au surface and undergoes oxidation. The nanoparticle is partially oxidized during each collision ($Ag = Ag^+ + e^-$), resulting in the Ag particle size decreasing with time. The arrows indicate the position of three clusters of collisions between the Ag particle and Au electrode.

Simulation Details. The initial position of each Ag nanoparticle in the simulation was chosen to be on the surface of the 12.5 μm diameter microdisk electrode. Thus, the simulated traces presented herein represent the nanoparticle dynamics beginning at the time of its first observable collision with the electrode. The nanoparticle diffusional flux to the disk microelectrode is largest at the electrode edge, which implies that a large percentage of the nanoparticles will undergo their first collision near the insulator/electrode edge. Therefore, to accurately compute the $i-t$ response of a real experiment, it is necessary to compute the initial positions of the particles. The different initial positions for each simulated nanoparticle were calculated on the basis of the landing probability for a microdisk electrode at a steady-state diffusive flux condition,[27] resulting in a distribution of starting positions that becomes denser from the center to the edge of the disk, as shown in Figure 3. Full details for the simulation of initial landing positions are provided in Supporting Information, section 4. It is clear from Figure 3 that many nanoparticles initially collide near the edge of the electrode. These particles have a higher probability of colliding only a few times, and then diffusing away from the electroactive Au surface without further oxidation. Conversely, the fewer nanoparticles that initially diffuse to the center of the Au electrode are likely to undergo more collisions.

The rules defining the simulations at $t > 0$ s can be broken down into those describing the random walk and those describing electrooxidation upon collision.

1. Random Walk Model. The Brownian motion of spherical particles in solution is described by the Einstein–Smoluchowski relationship between the one-dimensional particle step length, δx, and step time, τ,

$$\delta x^2 = 2D\tau \tag{1}$$

where D is the diffusion coefficient of the particle of radius r, as given by the Stokes–Einstein equation[1a]

$$D = \frac{k_B T}{6\pi\eta r} \tag{2}$$

In eq 2, k_B is the Boltzmann constant (1.381×10^{-23} J·K^{-1}), η is the viscosity of water (0.8937 mPa·s),[28] and T is the temperature (298.15 K). In the simulations, the Ag nanoparticle radius is initially set to 35 nm, corresponding to an initial diffusion coefficient of 7×10^{-8} cm^2 s^{-1}. We do not consider the possibility of near-wall hindered diffusion, which was incorporated into the model proposed by Long and coworkers.[24] In our model, the diffusion coefficient is assumed to obey eq 2 at all times and remain unaffected by the distance of the nanoparticle from the electrode surface.

Random walk models of the particle motion can be developed using the Stokes–Einstein relationship (eq 2) and arbitrary values of δx and τ that satisfy eq 1. This is the general approach used in the electrochemical literature to model

DOI: 10.1021/jacs.7b09842
J. Am. Chem. Soc. 2017, 139, 16923–16931

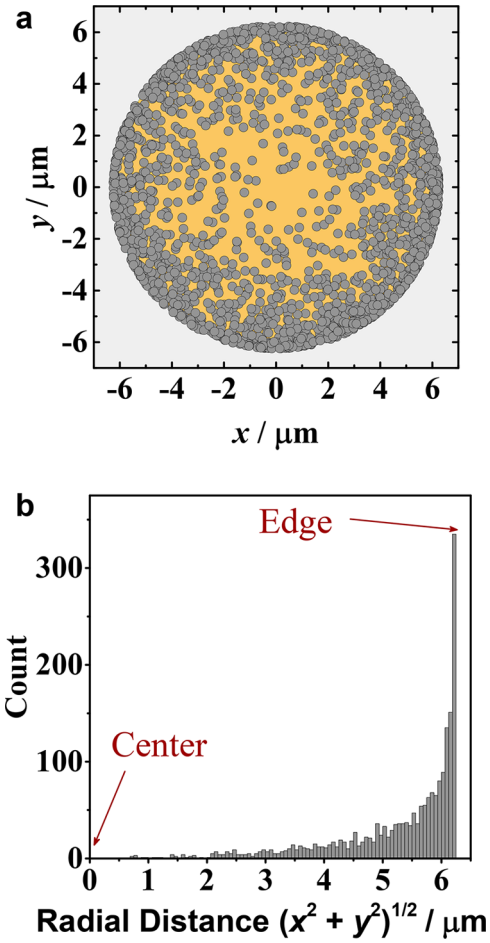

Figure 3. Initial collision positions of 2000 nanoparticles on a 12.5 μm diameter Au microdisk electrode randomly generated on the basis of their probability of arrival computed from Fick's laws of diffusion to a microdisk (see Supporting Information, section 4): (a) nanoparticle positions are shown as gray circles (not drawn to scale) on the Au electrode area shown, with x and y axes corresponding to position coordinates (x, y); (b) corresponding histogram along the radial distance from the electrode center with counts binned into 62.5 nm increments.

nanoparticle collision experiments.[16,24,26] Here, we use a method previously reported by our laboratory for describing electron-transfer kinetics based on the thermal velocity of the particle,[14b] allowing incorporation of the microscopic ET process with the motion of the particle.

The kinetic energy of the Ag nanoparticle is given by

$$\frac{1}{2}mv_x^2 = \frac{1}{2}mv_y^2 = \frac{1}{2}mv_z^2 = \frac{1}{2}k_BT \tag{3}$$

where m is the mass of the particle as calculated by

$$m = \rho_{Ag}\frac{4\pi r^3}{3} \tag{4}$$

with the density of Ag, $\rho_{Ag} = 10.49 \times 10^3$ kg·m^{-3}.[29] Variables ν_x, ν_y, and ν_z represent the thermal velocities of the nanoparticle in the x, y, and z directions. We assume isotropic motion and thus $\nu_x = \nu_y = \nu_z = \delta x/\tau$. For reference, the value of ν_x for a 35 nm radius Ag particle is 4.6 cm s^{-1}.

Equations 1–4 yield unique values for the δx and τ for the lattice random walk:

$$\delta x = \frac{2}{9}\sqrt{\frac{3k_BT\rho_{Ag}r}{\pi\eta^2}} \tag{5}$$

$$\tau = \frac{4\rho_{Ag}r^2}{9\eta} \tag{6}$$

The corresponding initial values of δx and τ are 0.30 nm and 6.4 ns, respectively, for a 35 nm radius particle. The radius of the particle, r, decreases upon oxidation, as described in the following section. Therefore, the values of δx, ν_x, and τ, all of which depend on r, also vary with time. For clarity, we do not explicitly indicate the time dependencies (e.g., $\tau(t)$) in the above notation. Further technical details of the random walk simulation are given in Supporting Information, section 5.

2. Particle Oxidation at the Electrode. The current density, j, corresponding to the rate of Ag electrodissolution, is taken as a constant over the course of the entire simulation time. Values of j in the range from 200 to 1500 A cm^{-2} were initially investigated to find the best fit to experimentally observed i–t traces such as those in Figure 1. This range of current density was estimated from literature values of the standard charge-transfer rate constant for Ag electrodissolution. The standard exchange current density, j_0^0, reported by Gerischer and Tischer for Ag/Ag$^+$ is 24 A cm^{-2}, with a transfer coefficient, α, of 0.65.[30] The standard exchange current density is related to the standard rate constant, k^0, by

$$j_0^0 = Fk^0C \tag{7}$$

where the concentration, C, is equal to $C_{Ag^+} = C_{Ag} = 10^{-3}$ mol cm^{-3}.[30d] This gives an effective standard rate constant, $k^0 = 0.25$ cm s^{-1}. We can roughly predict the current density for our conditions with no added Ag$^+$ ions using the typical Butler–Volmer formalism.[31]

$$j = Fk^0[C_{Ag^+(0,t)}e^{-\alpha f(E-E^{0\prime})} - C_{Ag(0,t)}e^{(1-\alpha)f(E-E^{0\prime})}] \tag{8}$$

Here $f = F/RT = 38.92$ V^{-1} and $E^{0\prime}$ is the formal potential, estimated using the standard potential for Ag/Ag$^+$ ($E^{0\prime} \approx E^0 = 0.799$ V). Because free Ag$^+$ is essentially absent for our conditions (see Supporting Information, section 6), C_{Ag}^+ was set to zero so the cathodic term vanishes. For a dissolution process, the effective concentration of Ag should be constant over time at the Ag metal–solution interface, so $C_{Ag(0,t)} = C_{Ag(0)}$. Because the standard exchange current density was determined by Gerischer assuming $C_{Ag} = 10^{-3}$ mol cm^{-3}, and we extracted k^0 from that value, the same standard C_{Ag} was used in eq 8 such that $C_{Ag(0,t)} = 10^{-3}$ mol cm^{-3}. Compton and co-workers also made this assignment in their kinetic model of Ag nanoparticle stripping voltammetry.[32] The standard rate constant determined to fit experimental Ag nanoparticle stripping peak potentials in that study was $k^0 = 1$ cm s^{-1}, on the same order of magnitude of our k^0 (0.25 cm s^{-1}). Under our experimental conditions of $E = 600$ mV vs Ag/AgCl wire (1.1 V vs SHE), eq 8 gives a current density of $j \sim 1400$ A cm^{-2} and a corresponding rate constant, k_{ox}, of ~15 cm s^{-1}. This value of j lies within the range of values used in the simulations presented below (200–1500 A cm^{-2}) that yield reasonable fits to the experimental analysis.

The charge transferred from the Ag nanoparticle to the Au electrode during a collision, Q_c, is computed as

DOI: 10.1021/jacs.7b09842
J. Am. Chem. Soc. 2017, 139, 16923–16931

$$Q_c = j \cdot 4\pi r^2 \cdot \tau \quad (9)$$

where $4\pi r^2$ is the surface area of the Ag nanoparticle immediately before a collision step. Here τ is the time of a random walk step as in eq 6, which only depends on the radius of the nanoparticle at the moment of collision. Thus, eq 9 can be simplified to a function of one dynamic variable, r, by combination with eq 6:

$$Q_c = j\frac{16\pi\rho_{Ag}}{9\eta}r^4 \quad (10)$$

Equation 10 indicates that the charge transferred per collision is a function of r^4, while all other terms remain constant as a function of time. The oxidation charge passed is then converted to a volume of Ag dissolved using Faraday's law (see Supporting Information, section 5, for details). The resulting smaller radius of the Ag nanoparticle sets the new values of δx and τ through eqs 5 and 6, which are then used to model the Brownian particle movements until the next collision.

The electrical charge and current due to charging of the Ag nanoparticle double layer upon collision are negligible and not included in the total charge or current reported here. For instance, assuming a double-layer capacitance of 20 μF cm^{-2},[31] we estimate a capacitive charge on the order of 1 fC if the potential of the Ag nanoparticle changes by ~0.5 V upon contact during the first collision with the Au electrode. Each subsequent collision of the charged nanoparticle will result in even smaller double layer charging. This magnitude of charge is too small to have any noticeable effect on the simulated and experimental $i-t$ traces.

3. Calculation of Simulated Current at Experimental Sampling Rate. In our experimental measurements of Ag nanoparticle collisions, data were sampled at 50 kHz, i.e., one data point per 20 μs, and processed with a three-pole Bessel filter of 10 kHz frequency to decrease noise. To allow quantitative comparison to experimental data, the simulated data in this work are reported at the same sampling rate and filter frequency. The calculated currents associated with each collision were first binned together in 4 μs intervals (250 kHz binning frequency), then filtered at 10 kHz with a three-pole Bessel filter function, and binned again at a sampling rate of 50 kHz. A more detailed description of the filtering protocol is provided in the Supporting Information, section 10.

RESULTS

Brownian dynamics simulations were performed individually for 2000 particles with initial positions at the electrode surface, as shown by Figure 3; the trajectory of each particle was determined for a period of 100 ms. Figure 4 shows the trajectories of three particles where the start point on the electrode surface (S) and end point (E) are labeled (further example traces for 17 additional particles are presented in Supporting Information, section 7). Each particle undergoes ~2 × 10^7 discrete movements, each less than 0.3 nm in the 100 ms period. Thus, it is impossible to resolve each step by visual inspection of the figure. In most cases, the Ag nanoparticles diffuse away from the electrode within 80 ms of its first collision with the surface. Particle 1, for example, travels about 1 μm away from the plane of the electrode after 100 ms. Before leaving the vicinity of the electrode, the Ag nanoparticle radius decreased from 35.4 to 31.6 nm, a consequence of 1310

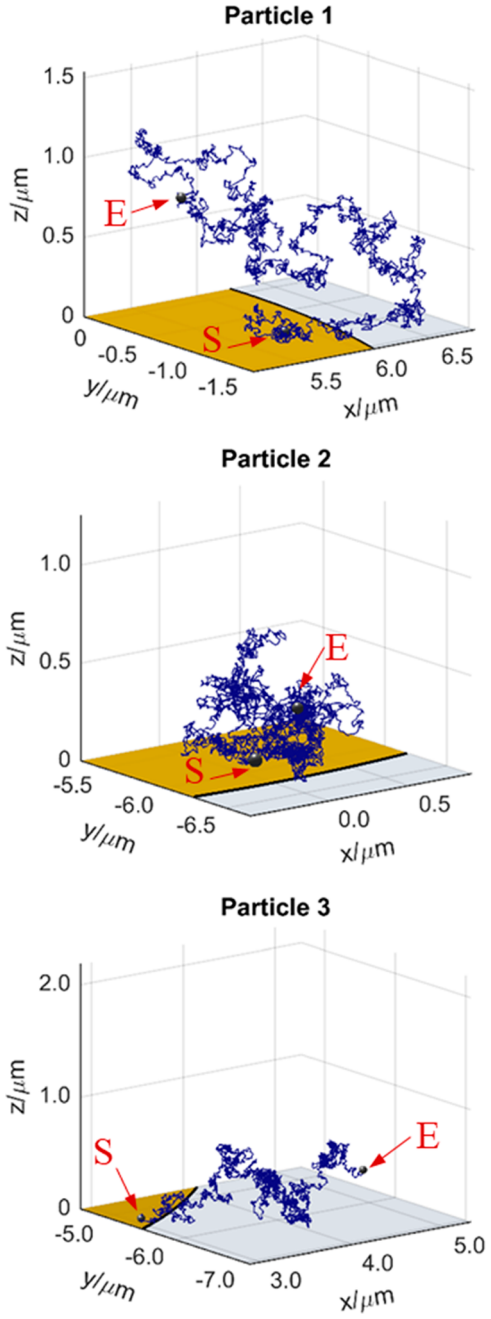

Figure 4. Three examples of 100 ms simulated trajectories of a Ag nanoparticle undergoing multicollision partial oxidations at j = 500 A cm^{-2} over a region of a 12.5 μm diameter Au microdisk electrode, as shown in yellow at the z = 0 μm plane and centered at x = 0 and y = 0 μm. The gray region at z = 0 μm represents the glass sheath. The start and end positions are marked by S and E. Nanoparticles at S and E positions (small gray spheres) are drawn to scale. (The traces in this figure correspond to particles 1, 2, and 3 in Figures 5 and 6.)

concurrent collision and electrooxidation events at the Au surface.

During the random walk, the particle collides with the electrode many times (average of ~2000 collisions for each simulation over the course of 100 ms, based on 2000 individual particle simulations). Each collision results in the oxidation/dissolution of a small portion of the particle and a contribution to the simulated current. Figure 5 presents the resulting $i-t$ curves (black lines) and $r-t$ curves (red lines) for the

DOI: 10.1021/jacs.7b09842
J. Am. Chem. Soc. 2017, 139, 16923−16931

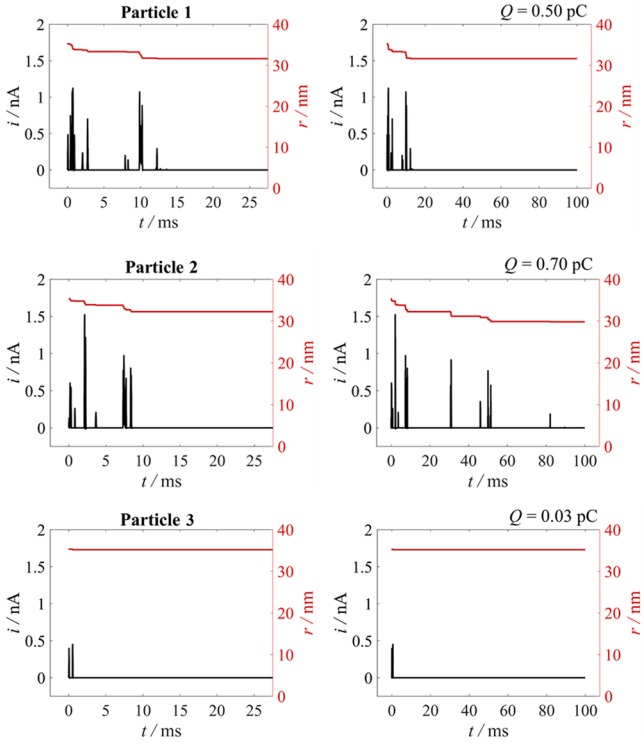

Figure 5. Simulated $i-t$ (black line) and $r-t$ (red line) curves for three different Ag nanoparticles, j = 500 A cm^{-2}, simulated with 20 μs sampling intervals (50 kHz sampling rate). The first 25 ms of each trace is shown in the left panel, and the full 100 ms time scale is provided in the right panel. The corresponding total charge from integrated Ag oxidation peaks over 100 ms, Q, is present in the right panel. Further example traces are shown in Supporting Information, section 8.

simulations presented in Figure 4 (17 additional examples are shown in Supporting Information, section 8). For each particle in Figure 5, a burst of current peaks with amplitudes of the order of 1 nA is observed toward the start of the 100 ms time window. Analogous to experimental $i-t$ traces, the exact current amplitude and temporal distribution of $i-t$ peak events are unique for each nanoparticle, a general indication of the stochastic nature of particle motion. The corresponding change in the particle radius is shown by the red line that decreases in a stepwise manner, as expected by the pulsatile nature of the current.

The general pattern of decreasing peak amplitude with time, observed in the majority of experimentally recorded events (Figure 1), is also apparent in the simulated $i-t$ plots in Figure 5. This pattern arises due to both decreasing nanoparticle size and decreasing simulation time step, τ, as the nanoparticle is oxidized; both processes lead to a decreasing quantity of charge transferred per collision according to eqs 8−10.

The total charge accumulated over the 100 ms simulation of each nanoparticle, Q, is shown in the top right-hand corner of the panels in Figure 5, and ranges from 0.03 to 0.7 pC. In contrast, complete oxidation of a 35 nm radius Ag nanosphere corresponds to 1.7 pC. Thus, the nanoparticles in Figure 5 are incompletely oxidized in the 100 ms time scale, in agreement with experimental observations. At the current density used in these examples (j = 500 A cm^{-2}), out of a total of 2000 particles, only 4 of the nanoparticle paths led to over 90% oxidation of the particle while 533 of the particles were <10% oxidized.

Particle 3 demonstrates an effect of initially landing near the electrode edge, as shown in Figure 4. The particle undergoes oxidation at the electrode during the first millisecond to transfer 30 fC of faradaic charge (Figure 5), signifying ∼1.9 × 10^5 Ag atoms oxidized (∼2% of the particle's mass), before diffusing beyond the electrode bounds. Upon subsequent encounters with the surface, particle 3 only collides with the glass sheath region (Figure 4) and therefore does not react further to generate current in the remaining 99 ms of the simulation (Figure 5). Particles 15 and 17 of Supporting Information, sections 7−9, also briefly interact with the electrode surface for a period of ∼1 ms and spend the remaining time away from the electrode surface.

Figure 6 shows the z-trajectories and the number of collisions per sampling interval (20 μs) corresponding to the three

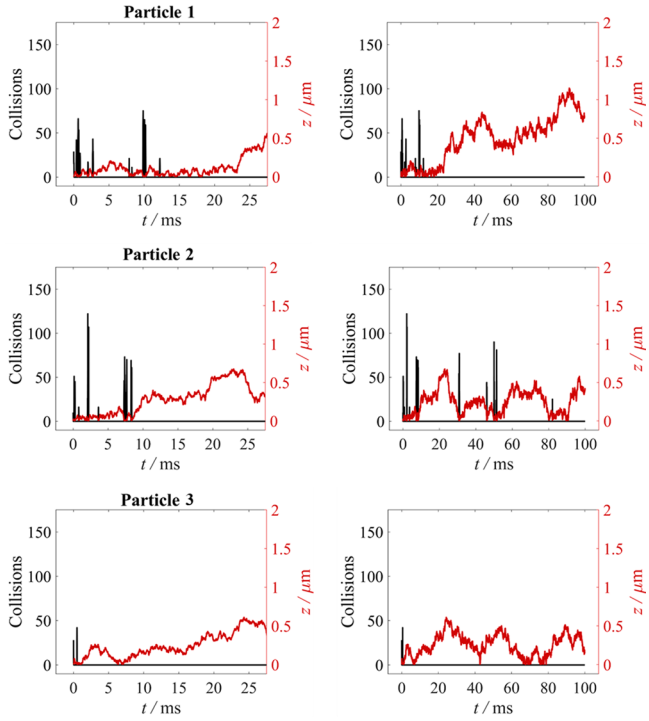

Figure 6. Collision count per 20 μs sampling interval and corresponding z coordinate, for three Ag nanoparticles (same as shown in Figure 5) repeatedly colliding with a 12.5 μm diameter electrode and undergoing multiple oxidation events. Further example traces are shown in Supporting Information, section 9.

particles in Figure 5. It can be seen from Figure 6 that the current in Figure 5 results from about 10−100 collisions of the particle with the electrode during the 20 μs sampling intervals, corresponding to collision frequencies in the range from 0.5 to 5 MHz. Individual collisions in this frequency range are not resolvable using the 10 kHz filter in amperometric experiments, nor here in the simulations where an identical 10 kHz filter is implemented. For the same reason, the instantaneous oxidation current that would result from a 500 A cm^{-2} current density at a 35 nm or smaller radius Ag nanosphere ($j \cdot 4\pi r^2$ = 75 nA) is not observable. The effect of filtering on the simulation results is presented and discussed in section 10 of the Supporting Information, including examples of $z-t$ and $i-t$ traces produced

DOI: 10.1021/jacs.7b09842
J. Am. Chem. Soc. 2017, 139, 16923−16931

Table 1. Average Values and Standard Deviations for the Maximum Peak Current, i_{max}, and Total Accumulated Charge, Q, for 100 ms Time Window Simulation of 2000 Ag Nanoparticle Oxidations[a]

	simulation, 2000 particles				
j (A·cm^{-2})	200	500	1000	1500	experiment, 166 particles E = 0.6 V vs Ag/AgCl wire
i_{max} (nA)	0.5 ± 0.2	1.1 ± 0.4	2.1 ± 0.7	3 ± 1	0.9 ± 0.7
Q (pC)	0.3 ± 0.2	0.5 ± 0.4	0.8 ± 0.5	1.0 ± 0.6	0.8 ± 0.5

[a]Each column represents a different current density, j, used in the simulation. Experimental results are included in the far-right column.

by sampling results at every simulation step as compared to filtered results.

Each individual current peak in the i–t trace results from tens to hundreds of collisions of a single particle with the electrode. In each case, there exist time intervals where no peak current is observed, which is indicative of periods when the particle has diffused into the bulk solution. Oftentimes the nanoparticle finds its way back to the electrode after one of these excursions to generate more oxidation peaks, usually smaller in magnitude. For example, in Figures 4, 5, and 6, particle 2 undergoes a burst of collisions in the first 10 ms, then diffuses in solution over a subsequent 20 ms interval, and finally returns to the electrode at ca. 30 ms. In contrast, particle 1 does not return to the electrode surface over the remaining time following its departure at $t \sim 13$ ms. Some particles hardly collide with the surface at all, whether electrode or insulating sheath. For example, particle 15 (see Supporting Information, section 9) only undergoes one burst of collisions with the electrode in the first 100 μs, never returning to the surface over the remaining time. All of the 2000 simulated particles were found to undergo at least one collision with the electrode (excluding the starting position at the electrode surface at t = 0 s). Thus, the probability of a nanoparticle undergoing at least one subsequent collision with the electrode over the 100 ms duration after its first collision at t = 0 s is essentially unity.

The maximum peak currents, i_{max}, and the total charge integrated over the 100 ms time interval, Q, were calculated for a set of 2000 nanoparticle simulations for each current density; their mean values and standard deviations are listed in Table 1. The peak currents and integrated charges increase with current density, as expected. The results indicate that the average current density associated with the observed i–t response during Ag nanoparticle collisions lies within the range from 500 to 1000 A cm^{-2}, corresponding to a k_{ox} ranging from 5 to 10 cm s^{-1}.

Figure 7a shows how the cumulative charge due to Ag nanoparticle oxidation, Q, increases as a function of time for different current densities. The shapes of the curves indicate that the average Ag nanoparticle dissolution rate decreases with time and approaches a plateau after a few tens of ms. This limit occurs because the overall probability of returning to the electrode decreases as the average particle travels further away over time. The corresponding average number of cumulative electrode collisions for a single Ag nanoparticle is plotted in Figure 7b. On average, Ag nanoparticles collide more frequently with the electrode at higher current densities because its size decreases faster. As the nanoparticle radius decreases, its thermal velocity increases, which causes the probability of electrode collision to increase.

The charge passed during a single collision, Q_c, can be converted to the number of Ag atoms oxidized per nanoparticle collision, as shown by the solid line in Figure 8a, according to Faraday's law. The dashed line in Figure 8a shows the number of Ag *surface* atoms as a function of nanoparticle radius (see

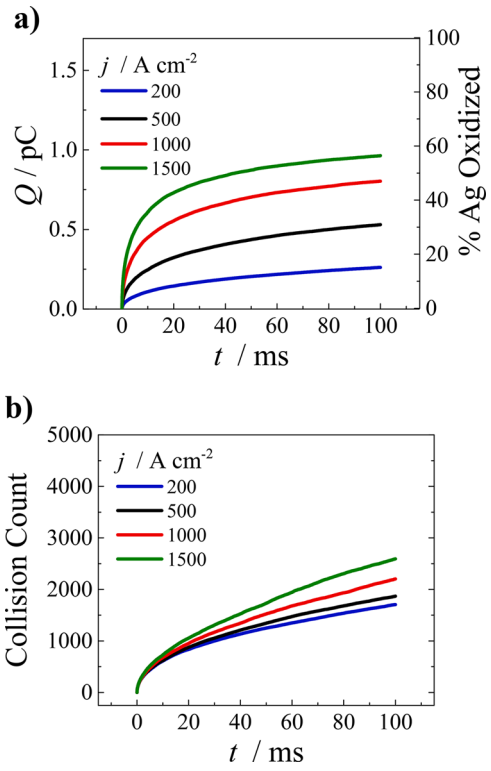

Figure 7. (a) Cumulative Q–t curves (calculated % Ag oxidized vs t also shown on the right y-axis) and (b) cumulative collision count vs t from averaged values of 2000 different Ag nanoparticle simulations for each current density, j, evaluated. Percentage of nanoparticle oxidation calculated by normalizing Q over the maximum calculated charge for complete oxidation of a 35 nm radius Ag sphere (Q/1.7 pC × 100%).

Supporting Information, section 11, for details on the estimation of surface atoms as a function of Ag nanoparticle radius). The amount of Ag oxidized per collision becomes smaller with decreasing nanoparticle radius because the area, $4\pi r^2$, and the collision duration, τ, both decrease as the nanoparticle becomes smaller.

Figure 8b shows the corresponding *percentage of Ag surface atoms* oxidized in a single collision as a function of nanoparticle radius. The curve indicates that the number of surface atoms oxidized in a single collision for a 35 nm radius particle represents ~1% of the total *surface* atoms available. The effect of a radius-dependent duration of charge transfer per collision is responsible for the predicted trend of decreasing % surface atoms oxidized per collision as a function of particle radius. For a nanoparticle of 5 nm radius, only one Ag atom on average is predicted to oxidize per collision. The simulation model suggests that nanoparticle sizes smaller than 5 nm radius may require more than one collision with the electrode to oxidize a single surface atom. For instance, a 0.75 nm radius Ag nanoparticle (containing ~100 Ag atoms) is estimated to

DOI: 10.1021/jacs.7b09842
J. Am. Chem. Soc. 2017, 139, 16923–16931

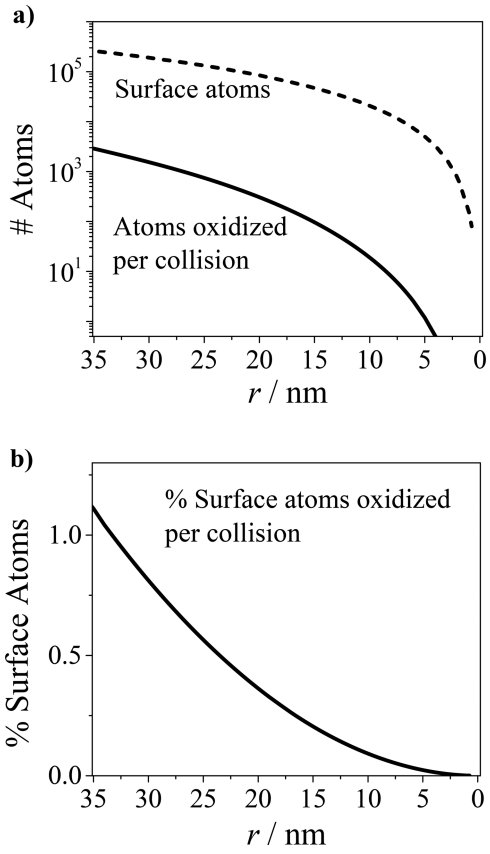

Figure 8. (a) Number of surface Ag atoms (dashed line) and number of Ag atoms oxidized in a single collision (solid line) following eq 10, j = 500 A cm^{-2}, shown on a logarithmic scale. (b) Percentage of surface atoms oxidized in a single collision as a function of nanoparticle radius.

require approximately 1700 collisions with the electrode to achieve oxidative dissolution of a single Ag surface atom.

As discussed earlier, the standard rate constant, k^0, we employed for the half-reaction, Ag ↔ Ag$^+$ + e$^-$, is ∼0.25 cm s^{-1} based on Gerischer's reported standard exchange current density. The mechanism for Ag electrodissolution and deposition was elucidated experimentally by Gerischer and Tischer in the 1950s using potential-step and double-pulse methods.[30a,b] Their proposed rate-limiting step for Ag dissolution is the detachment of Ag atoms from kink sites on the surface, prior to Ag adatom oxidation.[30a,33] Referring back to Figure 8b, our simulation model suggests that a 35 nm radius Ag nanoparticle will transfer 1% of its surface atoms into solution while in contact with the electrode for a few nanoseconds, as defined by τ. Interestingly, Gerischer measured the concentration of Ag adatom intermediates for the Ag/Ag$^+$ exchange reaction and concluded that they constitute roughly 1−4% of the surface of polycrystalline silver at 25 °C.[30b] Our results thus are quantitatively consistent with the Gerisher model, and suggest that a large portion of adatoms on the Ag nanoparticle undergo dissolution at the instantaneous moment of collision.

CONCLUSIONS

The lattice random-walk simulations of the motion of an individual Ag nanoparticle presented here quantitatively capture the recently reported multipeak i−t response observed in electrochemical collision experiments recently reported by Unwin,[25] Long,[24] and our laboratory.[20a] Specifically, the simulations predict the three key observables: (1) the magnitude of peak currents, (2) the overall duration of individual particle−electrode interaction (∼25 ms) and temporal pattern of the current peaks, and (3) the degree of particle oxidation. Our simulations are based on the mass-dependent thermal velocity of the Ag nanoparticle, which indicates that hundreds to thousands of individual nanosecond time scale collisions occur when a particle encounters the Au microelectrode, prior to the particle diffusing away into solution. In our current model, we have ignored effects of interfacial forces[34] that might drive particle motion (e.g., electric fields due to surface charge and to local Ag$^+$ generation), which we previously qualitatively proposed in our prior report to be responsible for the Ag nanoparticle not adhering to the Au electrode upon collision.

Quantitative comparison of the simulations with experiment allows us to estimate a Ag oxidation current density ranging from 500 to 1000 A cm^{-2} at 1.1 V vs SHE, corresponding to an ET transfer rate constant of ∼5−10 cm s^{-1}. While our ET model is admittedly overly simplified (e.g., we do not account for a distance-dependent ET from the Au electrode to the Ag nanoparticle, as considered by Long,[24] or the effect on tunneling currents due to the large density of states in the Ag nanoparticle[35]), the results strongly suggest that the ET rate for Ag nanoparticle oxidation is limited by the thermally driven motion of the nanoparticle. The thermal velocity ($(k_BT/m)^{1/2}$, eq 3) of the 35 nm radius Ag particles used in this study is equal to 4.6 cm s^{-1}, which is very close to our estimate of the ET rate (5−10 cm s^{-1}). Not coincidentally, we note that the thermal velocity is comparable to the heterogeneous collision rate constant derived from the Maxwell−Boltzmann distribution,[36] $Z_{het} = (k_BT/2\pi m)^{1/2}$, originally adopted by Marcus as a pre-exponential term in his theoretical expression for the ET rate constant for a unimolecular outer-sphere electron transfer at an electrode surface.[37] This "collision number" pre-exponential factor was later supplanted for small molecule redox systems by a pre-equilibrium complex formulation including the nuclear frequency factor, where the frequency is related to the vibrational modes of the solvent or intramolecular bonds of the reactant.[31,38] However, the collision frequency of Ag nanoparticles (which are massive relative to simple redox molecules) is much lower than the frequency of such vibrational modes. For such heavy redox-active nanoparticles, the collisional number model for the pre-exponential factor seems to be more appropriate for describing the ET kinetics of nanoparticle collision.

ASSOCIATED CONTENT

Supporting Information

The Supporting Information is available free of charge on the ACS Publications website at DOI: 10.1021/jacs.7b09842.

Further experimental and simulation details, supplemental example experimental i−t traces, Ag nanoparticle stripping voltammetry, supplemental simulated nanoparticle trajectories, supplemental simulated i−t and r−t traces, supplemental simulated collision count and z-position vs time traces, estimation of surface atom number, and references (PDF)

DOI: 10.1021/jacs.7b09842
J. Am. Chem. Soc. 2017, 139, 16923−16931

AUTHOR INFORMATION

Corresponding Authors

*zhang@chem.washington.edu
*white@chem.utah.edu

ORCID

Donald A. Robinson: 0000-0003-4531-0806
Martin A. Edwards: 0000-0001-8072-361X
Bo Zhang: 0000-0002-1737-1241
Henry S. White: 0000-0002-5053-0996

Author Contributions

‖D.A.R., Y.L.: These authors contributed equally.

Notes

The authors declare no competing financial interest.

ACKNOWLEDGMENTS

This work was funded by Air Force Office of Scientific Research MURI FA9550-14-1-0003 and the China Scholarship Council (201506275068).

REFERENCES

(1) (a) Einstein, A. *Investigations on the Theory of the Brownian Movement*; Dover Publications, Inc.: New York, 1956. (b) Brown, R. *Philos. Mag.* **1828**, *4*, 161. (c) von Smoluchowski, M. *Ann. Phys.* **1906**, *326*, 756.

(2) (a) Van Kampen, N. G. *Stochastic Processes in Physics and Chemistry*; Elsevier Science: Amsterdam, The Netherlands, 1992. (b) Chandrasekhar, S. *Rev. Mod. Phys.* **1943**, *15*, 1.

(3) Codling, E. A.; Plank, M. J.; Benhamou, S. *J. R. Soc., Interface* **2008**, *5*, 813.

(4) (a) Perrin, J.; Soddy, F. *Brownian Movement and Molecular Reality*; Dover Publications: New York, 2005. (b) Svedberg, T. *Z. Elektrochem. Angew. Phys. Chem.* **1906**, *12*, 853. (c) Zsigmondy, R.; Alexander, J. *Colloids and the Ultramicroscope: A Manual of Colloid Chemistry and Ultramicroscopy*; J. Wiley & Sons: New York, 1909.

(5) Einstein, A. *Z. Elektrochem. Angew. Phys. Chem.* **1907**, *13*, 41.

(6) Li, T.; Kheifets, S.; Medellin, D.; Raizen, M. G. *Science* **2010**, *328*, 1673.

(7) Huang, R.; Chavez, I.; Taute, K. M.; Lukic, B.; Jeney, S.; Raizen, M. G.; Florin, E.-L. *Nat. Phys.* **2011**, *7*, 576.

(8) Xiao, X.; Bard, A. J. *J. Am. Chem. Soc.* **2007**, *129*, 9610.

(9) (a) Kleijn, S. E. F.; Lai, S. C. S.; Miller, T. S.; Yanson, A. I.; Koper, M. T. M.; Unwin, P. R. *J. Am. Chem. Soc.* **2012**, *134*, 18558. (b) Guo, Z.; Percival, S. J.; Zhang, B. *J. Am. Chem. Soc.* **2014**, *136*, 8879.

(10) (a) Xiao, X.; Pan, S.; Jang, J. S.; Fan, F.-R. F.; Bard, A. J. *J. Phys. Chem. C* **2009**, *113*, 14978. (b) Dasari, R.; Robinson, D. A.; Stevenson, K. J. *J. Am. Chem. Soc.* **2013**, *135*, 570. (c) Kim, J.; Kim, B.-K.; Cho, S. K.; Bard, A. J. *J. Am. Chem. Soc.* **2014**, *136*, 8173. (d) Jung, A. R.; Lee, S.; Joo, J. W.; Shin, C.; Bae, H.; Moon, S. G.; Kwon, S. J. *J. Am. Chem. Soc.* **2015**, *137*, 1762. (e) Chen, C.-H.; Ravenhill, E. R.; Momotenko, D.; Kim, Y.-R.; Lai, S. C. S.; Unwin, P. R. *Langmuir* **2015**, *31*, 11932. (f) Castañeda, A. D.; Alligrant, T. M.; Loussaert, J. A.; Crooks, R. M. *Langmuir* **2015**, *31*, 876.

(11) (a) Kwon, S. J.; Bard, A. J. *J. Am. Chem. Soc.* **2012**, *134*, 7102. (b) Boika, A.; Thorgaard, S. N.; Bard, A. J. *J. Phys. Chem. B* **2013**, *117*, 4371. (c) Park, J. H.; Boika, A.; Park, H. S.; Lee, H. C.; Bard, A. J. *J. Phys. Chem. C* **2013**, *117*, 6651. (d) Kleijn, S. E. F.; Serrano-Bou, B.; Yanson, A. I.; Koper, M. T. M. *Langmuir* **2013**, *29*, 2054. (e) Tschulik, K.; Compton, R. G. *Phys. Chem. Chem. Phys.* **2014**, *16*, 13909. (f) Robinson, D. A.; Yoo, J. J.; Castañeda, A. D.; Gu, B.; Dasari, R.; Crooks, R. M.; Stevenson, K. J. *ACS Nano* **2015**, *9*, 7583. (g) Robinson, D. A.; Kondajji, A. M.; Castañeda, A. D.; Dasari, R.; Crooks, R. M.; Stevenson, K. J. *J. Phys. Chem. Lett.* **2016**, *7*, 2512.

(12) Wo, X.; Li, Z.; Jiang, Y.; Li, M.; Su, Y.-w.; Wang, W.; Tao, N. *Anal. Chem.* **2016**, *88*, 2380.

(13) Kang, M.; Perry, D.; Kim, Y.-R.; Colburn, A. W.; Lazenby, R. A.; Unwin, P. R. *J. Am. Chem. Soc.* **2015**, *137*, 10902.

(14) (a) Licht, S.; Cammarata, V.; Wrighton, M. S. *Science* **1989**, *243*, 1176. (b) White, R. J.; White, H. S. *Anal. Chem.* **2005**, *77*, 214 A A. (c) Bard, A. J.; Boika, A.; Kwon, S. J.; Park, J. H.; Thorgaard, S. N. *Nanoelectrochemistry*; CRC Press: Boca Raton, FL, 2015; p 241. (d) Singh, P. S.; Lemay, S. G. *Anal. Chem.* **2016**, *88*, 5017.

(15) (a) Amatore, C.; Grün, F.; Maisonhaute, E. *Angew. Chem., Int. Ed.* **2003**, *42*, 4944. (b) Cutress, I. J.; Dickinson, E. J. F.; Compton, R. G. *J. Electroanal. Chem.* **2011**, *655*, 1. (c) Kätelhön, E.; Krause, K. J.; Singh, P. S.; Lemay, S. G.; Wolfrum, B. *J. Am. Chem. Soc.* **2013**, *135*, 8874.

(16) Dickinson, E. J. F.; Rees, N. V.; Compton, R. G. *Chem. Phys. Lett.* **2012**, *528*, 44.

(17) White, R. J.; White, H. S. *Langmuir* **2008**, *24*, 2850.

(18) Huang, K.-C.; White, R. J. *J. Am. Chem. Soc.* **2013**, *135*, 12808.

(19) Andersen, O. S.; Feldberg, S. W. *J. Phys. Chem.* **1996**, *100*, 4622.

(20) (a) Oja, S. M.; Robinson, D. A.; Vitti, N. J.; Edwards, M. A.; Liu, Y.; White, H. S.; Zhang, B. *J. Am. Chem. Soc.* **2017**, *139*, 708. (b) Zhou, Y.-G.; Rees, N. V.; Compton, R. G. *Angew. Chem., Int. Ed.* **2011**, *50*, 4219.

(21) Patel, A. N.; Martinez-Marrades, A.; Brasiliense, V.; Koshelev, D.; Besbes, M.; Kuszelewicz, R.; Combellas, C.; Tessier, G.; Kanoufi, F. *Nano Lett.* **2015**, *15*, 6454.

(22) Brasiliense, V.; Patel, A. N.; Martinez-Marrades, A.; Shi, J.; Chen, Y.; Combellas, C.; Tessier, G.; Kanoufi, F. *J. Am. Chem. Soc.* **2016**, *138*, 3478.

(23) Batchelor-McAuley, C.; Ellison, J.; Tschulik, K.; Hurst, P. L.; Boldt, R.; Compton, R. G. *Analyst* **2015**, *140*, 5048.

(24) Ma, W.; Ma, H.; Chen, J.-F.; Peng, Y.-Y.; Yang, Z.-Y.; Wang, H.-F.; Ying, Y.-L.; Tian, H.; Long, Y.-T. *Chem. Sci.* **2017**, *8*, 1854.

(25) Ustarroz, J.; Kang, M.; Bullions, E.; Unwin, P. R. *Chem. Sci.* **2017**, *8*, 1841.

(26) Kwon, S. J.; Zhou, H.; Fan, F.-R. F.; Vorobyev, V.; Zhang, B.; Bard, A. J. *Phys. Chem. Chem. Phys.* **2011**, *13*, 5394.

(27) (a) Saito, Y. *Rev. Polarogr.* **1968**, *15*, 177. (b) Crank, J.; Furzeland, R. M. *IMA J. Appl. Math* **1977**, *20*, 355.

(28) Morrison, F. A. *An Introduction to Fluid Mechanics*; Cambridge University Press: Cambridge, U.K., 2013.

(29) Dean, J. A.; Lange, N. A. *Lange's Handbook of Chemistry*; McGraw-Hill: New York, 1999.

(30) (a) Gerischer, H.; Tischer, R. P. *Z. Elektrochem.* **1957**, *61*, 1159. (b) Gerischer, H. *Z. Elektrochem.* **1958**, *62*, 256. (c) Larkin, D.; Hackerman, N. *J. Electrochem. Soc.* **1977**, *124*, 360. (d) Hamann, C. H.; Hamnett, A.; Vielstich, W. *Electrochemistry*; Wiley: Weinheim, Germany, 1998.

(31) Bard, A. J.; Faulkner, L. R. *Electrochemical Methods: Fundamentals and Applications*; Wiley: New York, 2000.

(32) Ward Jones, S. E.; Campbell, F. W.; Baron, R.; Xiao, L.; Compton, R. G. *J. Phys. Chem. C* **2008**, *112*, 17820.

(33) Pinto, L. M. C.; Spohr, E.; Quaino, P.; Santos, E.; Schmickler, W. *Angew. Chem., Int. Ed.* **2013**, *52*, 7883.

(34) Peljo, P.; Manzanares, J. A.; Girault, H. H. *Chem. Sci.* **2017**, *8*, 4795.

(35) Chazalviel, J.-N.; Allongue, P. *J. Am. Chem. Soc.* **2011**, *133*, 762.

(36) Atkins, P.; de Paula, J. *Physical Chemistry*, 7th ed.; Freeman: New York, 2002.

(37) Marcus, R. *Annu. Rev. Phys. Chem.* **1964**, *15*, 155.

(38) (a) Sutin, N. *Acc. Chem. Res.* **1982**, *15*, 275. (b) Hupp, J. T.; Weaver, M. J. *J. Electroanal. Chem. Interfacial Electrochem.* **1983**, *152*, 1.

DOI: 10.1021/jacs.7b09842
J. Am. Chem. Soc. 2017, 139, 16923−16931